Eur. Phys. J. C 42, 73–87 (2005)
Digital Object Identifier (DOI) 10.1140/epjc/s2005-02262-5

THE EUROPEAN PHYSICAL JOURNAL C

The phase structure of lattice QCD with two flavors of Wilson quarks and renormalization group improved gluons

F. Farchioni[1], K. Jansen[2], I. Montvay[3,a], E. Scholz[3], L. Scorzato[4], A. Shindler[2], N. Ukita[3], C. Urbach[2,5], I. Wetzorke[2]

[1] Universität Münster, Institut für Theoretische Physik, Wilhelm- Klemm-Strasse 9, 48149 Münster, Germany
[2] NIC/DESY Zeuthen, Platanenallee 6, 15738 Zeuthen, Germany
[3] Deutsches Elektronen-Synchrotron DESY, Notkestr. 85, 22603 Hamburg, Germany
[4] Institut für Physik, Humboldt Universität zu Berlin, 12489 Berlin, Germany
[5] Freie Universität Berlin, Institut für Theoretische Physik, Arnimallee 14, 14196 Berlin, Germany

Received: 29 October 2004 / Revised version: 7 March 2005 /
Published online: 31 May 2005 –

Abstract. The effect of changing the lattice action for the gluon field on the recently observed [F. Farchioni, R. Frezzotti, K. Jansen, I. Montvay, G.C. Rossi, E. Scholz, A. Shindler, N. Ukita, C. Urbach, I. Wetzorke, Eur. Phys. J. C **39**, 421 (2005); hep-lat/0406039] first order phase transition near zero quark mass is investigated by replacing the Wilson plaquette action by the DBW2 action. The lattice action for quarks is unchanged: it is in both cases the original Wilson action. It turns out that Wilson fermions with the DBW2 gauge action have a phase structure where the minimal pion mass and the jump of the average plaquette are decreased, when compared to Wilson fermions with Wilson plaquette action at similar values of the lattice spacing. Taking the DBW2 gauge action is advantageous also from the point of view of the computational costs of numerical simulations.

1 Introduction

A basic feature of the low-energy dynamics in quantum chromodynamics (QCD) is the spontaneous chiral symmetry breaking implying the existence of light pseudo-Goldstone (pseudoscalar) bosons. The associated phase structure near zero quark masses has to be reproduced in the continuum limit by the lattice-regularized formulations but it is in general modified by lattice artifacts at non-vanishing lattice spacing. In lattice theories based on Wilson-type quark actions the possible phase structures have been investigated up to $\mathcal{O}(a^2)$ in the lattice spacing a by Sharpe and Singleton [2] in the framework of low-energy chiral Lagrangians [3,4] and using the effective continuum description of cut-off effects [5,6]. Their results allow for two possible "scenarios": the existence of the Aoki phase [7] or, alternatively, a first order phase transition near zero quark mass.

In a recent numerical simulation [1,8] the phase structure of lattice QCD with Wilson fermions and Wilson gauge action has been investigated with the help of the twisted mass Wilson fermion formulation [9,10]. For fixed values of a, smaller than $a \approx 0.2\,\mathrm{fm}$, evidence for a first order phase transition line, near zero quark mass in the plane of untwisted and twisted quark mass, has been found corresponding to the "second scenario" of [2]. It is important to remark that this line is finite and ends at a particular value of the twisted quark mass μ_c. This implies metastability and a non-zero minimum of the absolute value of quark- (and pion-) masses. These are lattice artifacts which are expected to vanish in the continuum limit where $\mu_c = 0$ and the first order phase transition line shrinks to a singular point. (For generalizations of the results of [2] for non-zero twisted mass see [11–13].) Considering, besides the bare quark masses, the bare gauge coupling, too, near the continuum limit the first order phase transition spans a surface, as it is schematically shown by Fig. 1.

It might be speculated that at the microscopic level the occurrence of the first order phase transition at $a > 0$ is accompanied by a massive rearrangement of small eigenvalues of the Wilson–Dirac operator. The detailed properties and, in particular, the strength of the first order phase transition does probably depend on the number and distribution of these eigenvalues. It is known that some type of small eigenvalues, especially real ones, are associated with small topological dislocations of the gauge field. A high probability of these dislocations and of the corresponding small eigenvalues is presumably a cut-off effect which can be diminished by an appropriate choice of the lattice action. In fact, it is known [14–17] that the small topological dislocations can, indeed, be suppressed by taking renormalization group improved (RGI) gauge actions as the Iwasaki action [18] or the DBW2 action [19].

[a] e-mail: montvay@mail.desy.de

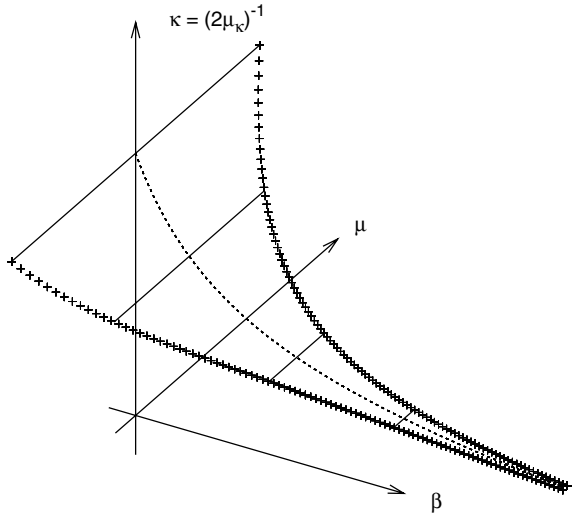

Fig. 1. The schematic view of the first order phase transition surface in the (β, κ, μ) space close to the continuum limit. (β is the bare gauge coupling, κ is the hopping parameter, μ is the bare twisted quark mass, $\mu_\kappa \equiv (2\kappa)^{-1}$ is the bare untwisted quark mass.) The crosses mark the second order boundary line of the first order phase transition surface. The strong coupling region near $\beta = 0$ is not shown in this figure

In the present paper we try to answer the question whether the combination of RGI gauge actions with the Wilson fermion action does shrink the first order phase transition line near zero quark mass. Here we restrict ourselves to the study of the DBW2 gauge action which has been successfully applied also in dynamical domain wall fermion simulations [20]. The goal of the present paper is to qualitatively show how a change of the gauge action will modify the phase structure. Hence, we do not aim here at a high precision study.

The Iwasaki action is often used in dynamical quark simulations by the CP-PACS and JLQCD Collaborations, in particular, in combination with the Sheikholeslami–Wohlert clover improved Wilson fermion action [6]. Earlier results of the JLQCD Collaborations indicate [21] that, indeed, a metastability seen in the average plaquette can be suppressed by replacing the Wilson plaquette action by the Iwasaki action. (See also [22], and for a review of earlier results on the phase structure of QCD, see [23]. An early discussion of the phase structure of QCD can also be found in [24].)

The plan of this paper is as follows: in the next section the lattice action and some parameters of the update algorithm are defined. In Sect. 3 we present the results of the numerical simulations. Section 4 is devoted to the investigation of the eigenvalue spectrum of the Wilson–Dirac operator near the origin. The last section contains some discussion and concluding remarks.

2 Lattice action and simulation algorithm

2.1 Lattice action

We apply for quarks the lattice action of Wilson fermions, which can be written as

$$S_q = \sum_x \left\{ \left(\overline{\chi}_x [\mu_\kappa + \mathrm{i}\gamma_5 \tau_3 \mu] \chi_x \right) - \frac{1}{2} \sum_{\mu=\pm 1}^{\pm 4} \left(\overline{\chi}_{x+\hat{\mu}} U_{x\mu} [r + \gamma_\mu] \chi_x \right) \right\} . \quad (1)$$

Here the ("untwisted") bare quark mass in lattice units is denoted by

$$\mu_\kappa \equiv a m_0 + 4r = \frac{1}{2\kappa} , \quad (2)$$

r is the Wilson parameter, set in our simulations to $r = 1$, am_0 is another convention for the bare quark mass in lattice units and κ is the conventional hopping parameter. In (1) the twisted mass μ is also introduced. $U_{x\mu} \in \mathrm{SU}(3)$ is the gauge link variable and we also defined $U_{x,-\mu} = U^\dagger_{x-\hat{\mu},\mu}$ and $\gamma_{-\mu} = -\gamma_\mu$.

For the SU(3) Yang–Mills gauge field we apply the DBW2 lattice action [19] which belongs to a one-parameter family of actions obtained by renormalization group considerations. These actions also include, besides the usual (1×1) Wilson loop plaquette term, planar rectangular (1×2) Wilson loops:

$$S_g = \beta \sum_x \left(c_0 \sum_{\mu<\nu;\, \mu,\nu=1}^{4} \left\{ 1 - \frac{1}{3} \mathrm{Re}\, U^{1\times 1}_{x\mu\nu} \right\} + c_1 \sum_{\mu\neq\nu;\, \mu,\nu=1}^{4} \left\{ 1 - \frac{1}{3} \mathrm{Re}\, U^{1\times 2}_{x\mu\nu} \right\} \right) , \quad (3)$$

with the normalization condition $c_0 = 1 - 8c_1$. (The notation $c_{0,1}$ is conventional. Of course, c_1 should not be confused with the parameter c_1 in the effective potential of [2,1].) The coefficient c_1 in (3) takes different values for various choices of RGI actions, for instance,

$$c_1 = \begin{cases} -0.331 & \text{Iwasaki action,} \\ -1.4088 & \text{DBW2 action.} \end{cases} \quad (4)$$

Clearly, $c_1 = 0$ corresponds to the original Wilson gauge action with the plaquette term only. Note that for $c_1 = -1/12$ one obtains the tree-level improved action in the Symanzik improvement scheme [25].

2.2 Twist angle

An important quantity is the twist angle ω, the polar angle in the plane of the untwisted and twisted mass (μ_κ, μ). We present here a method which allows one to determine the twist angle only on the basis of symmetry of the correlators defined in a given point of bare parameter space (see also [8]).

Following [10], we introduce the twist angle ω as the chiral rotation angle between the renormalized (physical) vector and axialvector currents $\hat{V}^a_{x\mu}$, $\hat{A}^a_{x\mu}$ and the bare bilinears of the χ-fields $V^a_{x\mu}$, $A^a_{x\mu}$:

$$V^a_{x\mu} \equiv \overline{\chi}_x \frac{1}{2}\tau_a\gamma_\mu\chi_x \ , \qquad A^a_{x\mu} \equiv \overline{\chi}_x \frac{1}{2}\tau_a\gamma_\mu\gamma_5\chi_x \ . \tag{5}$$

With the renormalization constants Z_V and Z_A we have

$$\hat{V}^a_{x\mu} = Z_V V^a_{x\mu} \cos\omega + \epsilon_{ab}\, Z_A A^b_{x\mu} \sin\omega \ , \tag{6}$$

$$\hat{A}^a_{x\mu} = Z_A A^a_{x\mu} \cos\omega + \epsilon_{ab}\, Z_V V^b_{x\mu} \sin\omega \, , \tag{7}$$

where only charged currents are considered ($a = 1, 2$).

The twist angle ω is related to the ratio of the renormalized twisted and untwisted masses entering the chiral Ward identities [10]. (In [10] this definition of the twist angle was called α.) We define, in addition, the two auxiliary angles

$$\begin{aligned} \omega_V &= \arctan(Z_A Z_V^{-1} \tan\omega) \ , \\ \omega_A &= \arctan(Z_V Z_A^{-1} \tan\omega) \ . \end{aligned} \tag{8}$$

In terms of ω_V, ω_A (6) and (7) are written as

$$\hat{V}^a_{x\mu} = \mathcal{N}_V \left(\cos\omega_V V^a_{x\mu} + \epsilon_{ab} \sin\omega_V A^b_{x\mu}\right) , \tag{9}$$

$$\hat{A}^a_{x\mu} = \mathcal{N}_A \left(\cos\omega_A A^a_{x\mu} + \epsilon_{ab} \sin\omega_A V^b_{x\mu}\right) \tag{10}$$

where the overall multiplicative renormalization is ($X = V, A$):

$$\mathcal{N}_X = \frac{Z_X}{\cos\omega_X \sqrt{1 + \tan\omega_V \tan\omega_A}} \ . \tag{11}$$

From (8) it follows that

$$\omega = \arctan\left(\sqrt{\tan\omega_V \tan\omega_A}\right) \ . \tag{12}$$

As shown by the relations in (8) and (12), the values of ω, ω_V and ω_A coincide for $|\omega| = 0, \pi/2$. However, for other angles they are, in general, different and the difference goes to zero in the continuum limit only as fast as $Z_V/Z_A \to 1$.

A possibility to determine ω_V and ω_A is to impose the vector and axialvector Ward identities, respectively, with a suitable insertion operator $\hat{O}_x$. For instance, in the vector case one can use the Ward identity

$$\sum_{\boldsymbol{x},\boldsymbol{y}} \langle \partial^*_\mu \hat{V}^+_{x\mu}\, \hat{O}^-_y \rangle = 0 \implies \tan\omega_V = \frac{-\mathrm{i}\sum_{\boldsymbol{x},\boldsymbol{y}} \langle \partial^*_0 V^+_{x0}\, \hat{O}^-_y \rangle}{\sum_{\boldsymbol{x},\boldsymbol{y}} \langle \partial^*_0 A^+_{x0}\, \hat{O}^-_y \rangle} \ . \tag{13}$$

Here the indices + and − refer to the charged components $\tau_\pm \equiv \tau_1 \pm \mathrm{i}\tau_2$ and ∂^*_μ denotes the backward lattice derivative.

Another possibility for determining the twist angles ω_V, ω_A and ω is to impose parity conservation for suitable matrix elements, for instance with the pseudoscalar density $P^\pm_x = \bar{\chi}_x \frac{\tau^\pm}{2}\gamma_5\chi_x$:

$$\sum_{\boldsymbol{x},\boldsymbol{y}} \langle \hat{A}^+_{x0}\, \hat{V}^-_{y0} \rangle \ = \ \sum_{\boldsymbol{x},\boldsymbol{y}} \langle \hat{V}^+_{x0}\, P^-_y \rangle \ = \ 0 \ . \tag{14}$$

These equations admit the solution

$$\tan\omega_V = \frac{-\mathrm{i}\sum_{\boldsymbol{x},\boldsymbol{y}} \langle V^+_{x0}\, P^-_y \rangle}{\sum_{\boldsymbol{x},\boldsymbol{y}} \langle A^+_{x0}\, P^-_y \rangle} \ , \tag{15}$$

$$\tan\omega_A = \frac{\mathrm{i}\sum_{\boldsymbol{x},\boldsymbol{y}} \langle A^+_{x0}\, V^-_{y0} \rangle + \tan\omega_V \sum_{\boldsymbol{x},\boldsymbol{y}} \langle A^+_{x0}\, A^-_{y0} \rangle}{\sum_{\boldsymbol{x},\boldsymbol{y}} \langle V^+_{x0}\, V^-_{y0} \rangle - \mathrm{i}\tan\omega_V \sum_{\boldsymbol{x},\boldsymbol{y}} \langle V^+_{x0}\, A^-_{y0} \rangle} \ . \tag{16}$$

In (14) one can also take the derivatives of the currents instead of the currents themselves. For instance, taking the divergence of the vector current in the second equality gives the same equations as (13) with $\hat{O} = P$.

Once ω_V and ω_A are determined, the twist angle ω can be obtained by (12). This method for determining the twist angle can also be used in case of simulations with partially quenched twisted mass quarks. The estimate of ω is, of course, affected by $\mathcal{O}(a)$ ambiguities. For non-zero twisted mass $\mu \neq 0$ the critical bare untwisted quark mass $\mu_\kappa = \mu_{\kappa_{\rm cr}}$, or the critical hopping parameter $\kappa_{\rm cr} = (2\mu_{\kappa_{\rm cr}})^{-1}$, is signaled by $|\omega| = \pi/2$.

2.3 Updating algorithm

Concerning updating in our numerical simulations, we apply the two-step multi-boson (TSMB) algorithm [26], which has been tuned to QCD simulations with Wilson quarks in previous works [1, 27–30]. (For details and references see in these papers.) In [27] there is an approximate formula for the computational cost of an update cycle in terms of matrix-vector-multiplications (MVMs):

$$\frac{N_{\rm MVM}}{\rm cycle} \ \simeq \ 6(n_{\rm B} n_1 N_\Phi + N_U) + 2 n_{\rm B}(n_2 + n_3) N_{\rm C} + I_{\rm G} F_{\rm G} \ . \tag{17}$$

Here $n_{1,2,3}$ are the orders of polynomials used in the two approximation steps, $n_{\rm B}$ gives the multiplicity in determinant breakup, N_Φ is the number of local bosonic sweeps per update cycle, N_U the number of local gauge sweeps, $N_{\rm C}$ the number of global Metropolis accept–reject correction steps, and $I_{\rm G}$ and $F_{\rm G}$ give the number of MVMs in the global boson heatbath and its frequency, respectively.

The number of MVMs can also be converted into the number of floating point operations by noting that in our code, for vanishing twisted mass, we have

$$1 \text{ MVM} \ \simeq \ 1.2 \cdot 10^3 \, \Omega \, \text{flop} \ , \tag{18}$$

where Ω is the number of lattice points. For non-zero twisted mass there is an additional factor 2 due to the flavor index. (This does, however, not mean that twisted mass fermions are a factor of two more expensive since in this case the two flavors are incorporated in one fermion matrix and the polynomial approximations have lower orders; see Appendix A.2 of [1].)

Measuring the integrated autocorrelations $\tau_{\rm int}$ as a function of the quark mass in lattice units am_q and of the lattice volume Ω, previous experience tells that one

can approximate the computational cost of a number of update cycles equal to $\tau_{\rm int}$ by the simple formula

$$C_{\tau_{\rm int}} \simeq F\,(am_q)^{-z}\,\Omega\ . \tag{19}$$

According to [27], in case of combining the Wilson fermion action with the Wilson plaquette gauge action, the power of the inverse quark mass is close to $z = 2$. The overall factor F depends on the quantity under investigation. For Wilson quarks with Wilson gauge action the previous results can be summarized, for instance, for the average plaquette and for the pion mass determined with a randomly chosen source by [30]

$$F_{\rm plaq} \simeq 7 \cdot 10^6\,{\rm flop}\ , \qquad F_{m_\pi} \simeq 10^6\,{\rm flop}\ . \tag{20}$$

Let us note that the approximate formula in (19) has been, up to now, verified only for some fixed values of the gauge coupling β. The β-dependence of F has not yet been systematically investigated.

3 Numerical simulation results

Our aim is to compare the phase structure of two-flavor ($N_f = 2$) QCD near zero quark mass for Wilson lattice fermion action and DBW2 gauge action with the one observed in [1,8] for Wilson fermion action and Wilson (plaquette) gauge action. Since the phase structure obviously depends on the lattice spacing, we have to find the values of the bare parameters (β, μ_κ) in the lattice action (1)–(3) which correspond to quark mass $m_q \simeq 0$ and to the same lattice spacing as in [1,8], namely $a \simeq 0.2\,{\rm fm}$. For having a fair comparison, the lattice volume has to be kept constant, too, because the metastability phenomenon does also depend on it. Therefore, we shall compare the results on $12^3 \times 24$ lattices.

A possibility for facilitating the parameter tuning is to explore the position of the high-temperature phase transition on lattices with time extension $N_t = 4$ and $N_t = 6$ for small quark masses, which mark $a = 0.25$–$0.30\,{\rm fm}$ and $a = 0.17$–$0.20\,{\rm fm}$, respectively. (This method with $N_t = 4$ has been applied, for instance, in [27].) A useful first orientation is also provided by the quenched studies. (For a useful collection of data on RGI gauge actions see [31] and references therein). For specifying the actual value of the lattice spacing we determine the Sommer scale parameter in lattice units r_0/a [32], which we set by definition to be $r_0 \equiv 0.5\,{\rm fm}$, independently from the quark mass.

In order to localize the $N_t = 4$ high-temperature phase transition we fixed the gauge coupling at $\beta = 0.55$ and changed the bare quark mass μ_κ (or, equivalently, the hopping parameter $\kappa = (2\mu_\kappa)^{-1}$). The results on an $8^3 \times 4$ lattice for the absolute value of the Polyakov line and average plaquette are given in Fig. 2. As it is shown by the figure, the transition with the DBW2 action is rather smooth, barely visible. This has to be contrasted with the strong and sudden increase of both Polyakov line and average plaquette in case of the Wilson plaquette action, which is also shown for comparison in Fig. 2.

Table 1. Bare couplings and parameters of the TSMB algorithm in runs with the DBW2 gauge action. The determinant breakup multiplicity is $n_{\rm B} = 4$ in all runs. Small letters label runs on $8^3 \times 16$ lattices at $\beta = 0.55$ whereas capital letters stand for runs on $12^3 \times 24$ lattices at $\beta = 0.67$. The suffix l and h denote "low" and "high" plaquette phase, respectively. Those runs with a calligraphic letter are performed with an additional twisted mass term ($\mu = 0.01$). The number of analyzed configurations is given in the last column. An asterix on these numbers denotes that a few configurations have very low ($\ll 1$) reweighting factors. The analyzed gauge configurations are separated by 10 update cycles, except for runs (a) and ($\mathcal{A}_{\rm l}$), where they are separated by 100 and 2 update cycles, respectively

run	κ	n_1	n_2	n_3	λ	ϵ	$N_{\rm conf}$
(a)	0.184	22	100	102	24	$2.4{\cdot}10^{-3}$	116
(b)	0.186	22	200	220	23	$5.8{\cdot}10^{-4}$	381
(c)	0.188	24	500	520	23	$5.7{\cdot}10^{-5}$	165
(d)	0.190	30	900	940	22	$1.1{\cdot}10^{-5}$	66*
(e)	0.192	30	1400	1440	22	$2.7{\cdot}10^{-6}$	159*
(f)	0.193	26	650	680	22	$2.7{\cdot}10^{-5}$	192
(g)	0.194	22	300	320	21	$2.1{\cdot}10^{-4}$	111
($A_{\rm l}$)	0.165	28	210	220	26	$1.3 \cdot 10^{-3}$	82
($C_{\rm l}$)	0.167	28	500	510	25	$1.3 \cdot 10^{-4}$	62
($C_{\rm h}$)	0.167	30	1100	1200	25	$1.3 \cdot 10^{-5}$	220
($D_{\rm l}$)	0.168	30	1100	1200	25	$1.2 \cdot 10^{-5}$	82*
($D_{\rm h}$)	0.168	30	1100	1200	25	$1.2 \cdot 10^{-5}$	211
($E_{\rm h}$)	0.170	28	900	920	24	$4.8 \cdot 10^{-5}$	194
($F_{\rm h}$)	0.172	28	500	510	24	$1.2 \cdot 10^{-4}$	151
($G_{\rm h}$)	0.175	28	500	510	23	$1.1 \cdot 10^{-4}$	78*
($\mathcal{A}_{\rm l}$)	0.165	16	250	270	24	$1.2 \cdot 10^{-3}$	540
($\mathcal{B}_{\rm l}$)	0.166	18	420	460	24	$3.6 \cdot 10^{-4}$	58
($\mathcal{C}_{\rm h}$)	0.167	18	420	460	24	$3.6 \cdot 10^{-4}$	139
($\mathcal{D}_{\rm h}$)	0.168	18	420	460	24	$3.6 \cdot 10^{-4}$	321
($\mathcal{E}_{\rm h}$)	0.170	18	420	460	24	$3.6 \cdot 10^{-4}$	100

A similar analysis on $12^3 \times 6$ lattices at $\beta = 0.67$ gives qualitatively similar results but there the difference between the DBW2 and the Wilson plaquette action is smaller because the transition for the Wilson plaquette action becomes weaker.

3.1 Results on an $8^3 \times 16$ lattice at $\beta = 0.55$

The runs on an $8^3 \times 16$ lattice at $\beta = 0.55$ and $\mu = 0$ were started from the low-temperature phase by taking four copies in the time direction of some of the $8^3 \times 4$ lattices. The parameters of these runs are specified in the first part of Table 1.

Besides the hopping parameter κ also some parameters of the TSMB updating algorithm are specified: the orders of the polynomials used $n_{1,2,3}$ and the interval covering the eigenvalues of the squared preconditioned hermitean quark matrix $[\epsilon, \lambda]$.

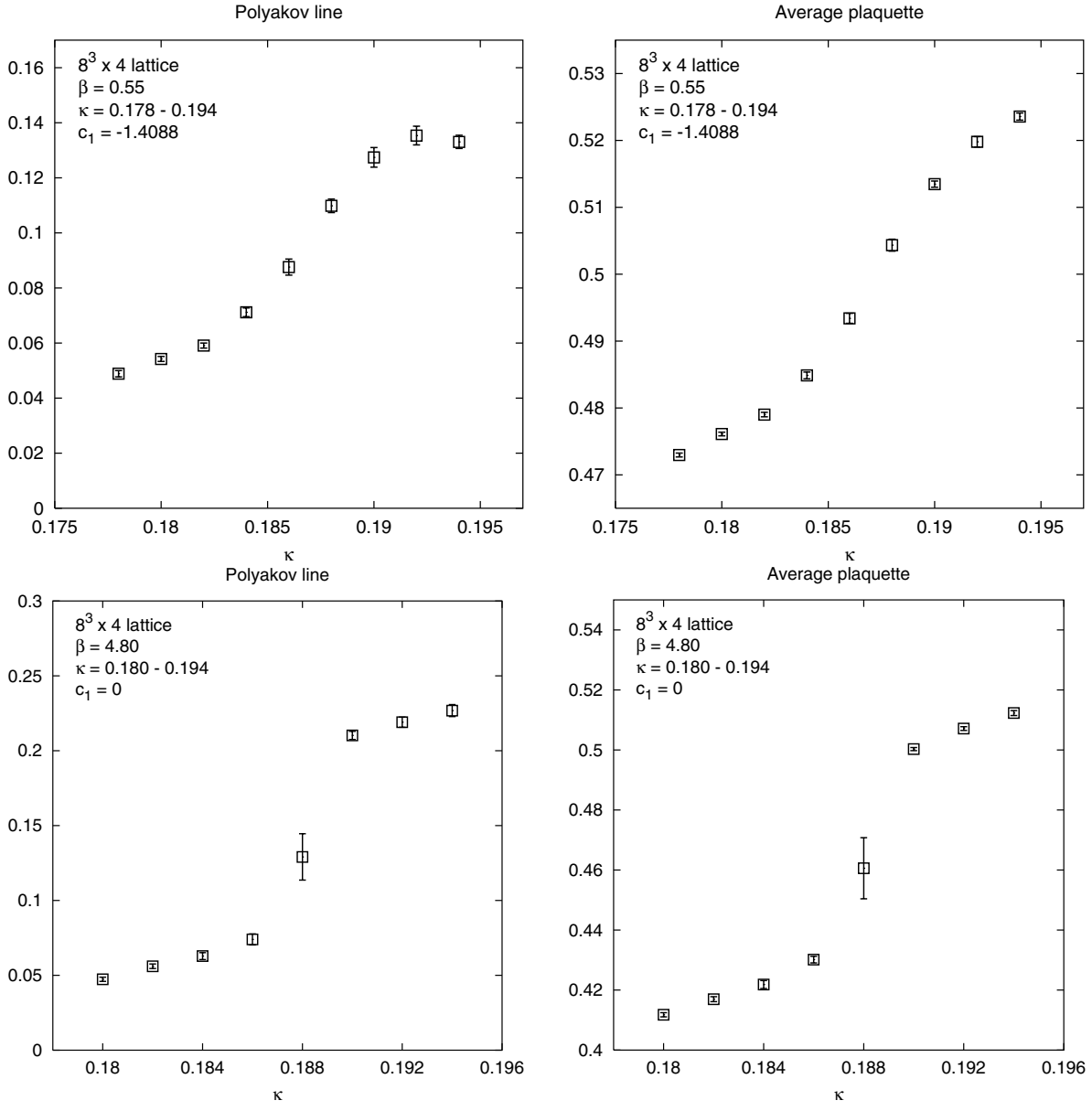

Fig. 2. Upper panels: the signals of the $N_t = 4$ non-zero temperature transition on an $8^3 \times 4$ lattice with the DBW2 gauge action. Lower panels: the same with Wilson gauge action. Left panels: absolute value of the Polyakov line, right panels: average plaquette, both as a function of κ

In the $8^3 \times 16$ runs we looked for signals of metastability but we did not find any. The results for some interesting quantities are collected in the first part of Table 2: the pion (i.e. pseudoscalar meson) and ρ-meson masses and the bare quark mass in lattice units $am_\chi^{\rm PCAC}$. Some of these quantities are also shown in Fig. 3. The scale parameter in lattice units r_0/a was also determined. We note in passing that at this small value of β and with our partly low statistics the evaluation of r_0 is rather difficult. Nevertheless, in order to estimate quantities also in physical units, we performed a purely statistical analysis for r_0, being aware of the fact that systematic effects can be large.

The bare quark mass $am_\chi^{\rm PCAC}$ is defined by the PCAC relation containing the axialvector current $A^a_{x\mu}$ in (5) and the pseudoscalar density insertion:

$$am_\chi^{\rm PCAC} \equiv \frac{\langle \partial^*_\mu A^+_{x\mu}\, P^-_y \rangle}{2\langle P^+_x\, P^-_y \rangle}\ . \tag{21}$$

Since for the moment we do not determine the Z-factors of multiplicative renormalization, the bare quark mass $am_\chi^{\rm PCAC}$ contains an unknown $\mathcal{O}(1)$ Z-factor $Z_q \equiv Z_P/Z_A$. In the following analysis we extracted the quark mass with the method detailed in [27]; see Sect. 3.1.1 there.

In agreement with the absence of a signal for metastability, the μ_κ-dependence of the pion mass and quark

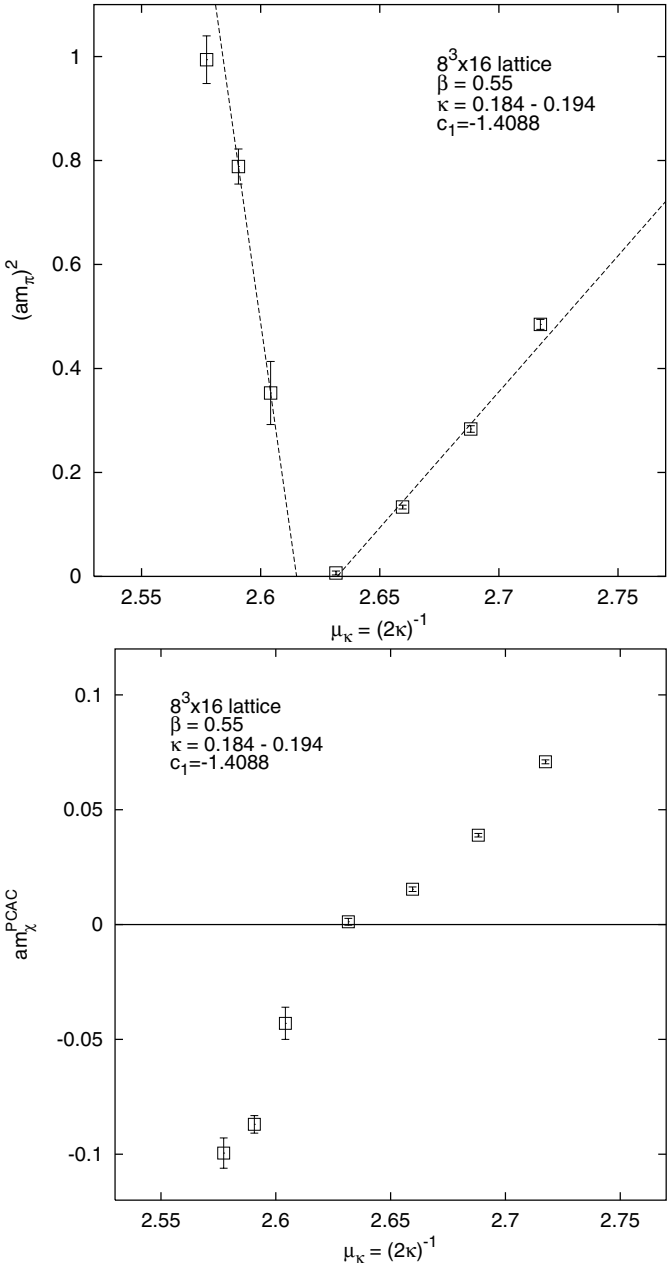

Fig. 3. Results of the numerical simulation on an $8^3 \times 16$ lattice at $\beta = 0.55$: upper panel the square of the pion mass $(am_\pi)^2$, lower panel the PCAC quark mass $am_\chi^{\rm PCAC}$. In the upper panel the dashed lines are extrapolations to zero pion mass: at the right it is a linear fit of four points, at the left a straight line connecting two points with small quark mass

mass in Fig. 3 is consistent with the absence of a first order phase transition at this gauge coupling ($\beta = 0.55$). A rough estimate for the value of the lattice spacing is $a \simeq 0.30\,\mathrm{fm}$ in the positive quark mass phase and $a \simeq 0.23\,\mathrm{fm}$ in the negative quark mass phase. The upper panel in Fig. 3 suggests the existence of a short interval ($\mu_\kappa \in [2.62, 2.63]$ or $\kappa \in [0.190, 0.191]$) of an Aoki phase near zero quark- and pion masses. This behavior is qualitatively similar to the one for the Wilson plaquette action which also shows the existence of the Aoki phase at strong gauge coupling [33].

Table 2. Results of runs specified in Table 1 for different quantities

run	am_π	am_ρ	m_π/m_ρ	$am_\chi^{\rm PCAC}$
(a)	0.6962(69)	1.0015(75)	0.6952(37)	0.07086(85)
(b)	0.5325(60)	0.9013(75)	0.5908(57)	0.03890(75)
(c)	0.3652(49)	0.840(26)	0.435(13)	0.0154(10)
(d)	0.081(24)	0.62(38)	0.130(78)	0.0012(15)
(e)	0.594(51)	1.80(30)	0.355(42)	−0.0430(70)
(f)	0.888(19)	1.794(30)	0.495(13)	−0.0870(38)
(g)	0.997(23)	1.820(59)	0.548(17)	−0.0995(66)
$(A_{\rm l})$	0.454(04)	0.724(25)	0.627(18)	0.0414(05)
$(C_{\rm l})$	0.343(07)	0.735(32)	0.466(21)	0.0222(11)
$(C_{\rm h})$	0.313(22)	0.776(125)	0.403(67)	−0.0222(28)
$(D_{\rm l})$	0.153(12)	0.445(109)	0.344(91)	0.0053(17)
$(D_{\rm h})$	0.380(31)	1.144(88)	0.332(37)	−0.0335(54)
$(E_{\rm h})$	0.644(15)	1.324(75)	0.487(27)	−0.0834(38)
$(F_{\rm h})$	0.840(23)	1.468(52)	0.572(25)	−0.1295(77)
$(G_{\rm h})$	1.005(44)	1.801(81)	0.558(28)	−0.1585(103)
$(\mathcal{A}_{\rm l})$	0.4641(45)	0.7228(58)	0.6421(53)	0.03803(81)
$(\mathcal{B}_{\rm l})$	0.341(05)	0.634(55)	0.538(45)	0.0177(22)
$(\mathcal{C}_{\rm h})$	0.291(12)	0.607(232)	0.480(178)	−0.0149(22)
$(\mathcal{D}_{\rm h})$	0.472(07)	1.035(72)	0.456(32)	−0.0469(16)
$(\mathcal{E}_{\rm h})$	0.712(14)	1.136(65)	0.627(34)	−0.0946(72)

3.2 Results on a $12^3 \times 24$ lattice at $\beta = 0.67$

With a short investigation of the high-temperature phase transition on a $12^3 \times 6$ lattice one can easily localize the gauge coupling β and bare quark mass $\mu_\kappa = (2\kappa)^{-1}$ where the lattice spacing is about a factor 3/2 smaller than at $\beta = 0.55$. It turned out that one can take $\beta = 0.67$ and $\kappa \simeq 0.17$. Fixing $\beta = 0.67$ and changing κ we performed several runs on a $12^3 \times 24$ lattice. In this way the physical volume of the lattice is approximately the same as the one of an $8^3 \times 16$ lattice at $\beta = 0.55$. In order to be able to compare with the results of [1], besides the runs with $\mu = 0$, at this β we also considered a non-vanishing twisted mass $\mu = 0.01$.

First we looked also here at $\mu = 0$ for a signal of metastability in the average plaquette and we found it near $\kappa = 0.167$–0.168, as it is shown by the upper panel of Fig. 4. Note that the average plaquette values are substantially higher here than at $\beta = 5.2$ with the Wilson plaquette gauge action in [1]: $A_{\rm plaq} \equiv \langle \frac{1}{3} \mathrm{Re}\,\mathrm{Tr}\, U_{\rm plaq} \rangle \simeq 0.59$ instead of $A_{\rm plaq} \simeq 0.52$. This qualitatively shows that the gauge field with DBW2 is smoother.

We also determined the pion, ρ-meson and quark masses, with the results given in Table 2. (For a graphical representation of some of these results see also the upper panels of Fig. 5.) For the extraction of r_0/a we performed

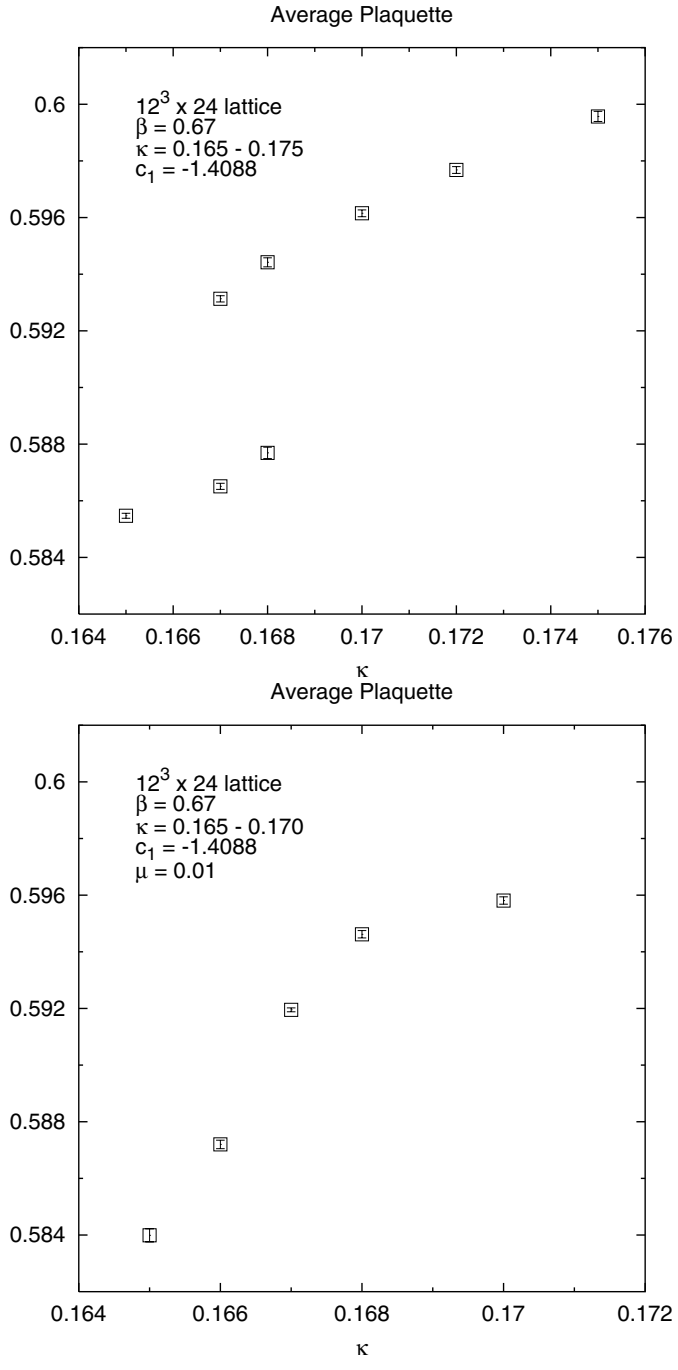

Fig. 4. The average plaquette at $\beta = 0.67$ on a $12^3 \times 24$ lattice as a function of the hopping parameter κ: upper panel $\mu = 0$ and lower panel $\mu = 0.01$, respectively

only a statistical analysis also here, neglecting the systematic effects. Let us give a range of values for the runs in Table 2. For A_l to D_l we find $2.37 < r_0/a < 2.76$ in the low and for C_h to G_h $2.72 < r_0/a < 3.17$ in the high plaquette phases, respectively. For $\mathcal{A}_\mathrm{l}, \mathcal{B}_\mathrm{l}$ we find $2.39 < r_0/a < 2.54$ in the low and for $\mathcal{C}_\mathrm{h}$ to $\mathcal{E}_\mathrm{h}$ we find $2.89 < r_0/a < 3.07$ in the high plaquette phase.

From the values of the scale parameter r_0/a we determined the lattice spacing, and found $a \simeq 0.18$–$0.21\,\mathrm{fm}$ in the positive and $a \simeq 0.16$–$0.18\,\mathrm{fm}$ in the negative quark mass phase, respectively. This is quite close to the values obtained in both phases with the Wilson plaquette gauge action at $\beta = 5.2$ in [1].

Going to the positive twisted mass $\mu = 0.01$, the metastability in the average plaquette disappears on our $12^3 \times 24$ lattice, as it is shown by the lower panel of Fig. 4. Having in mind the strong metastability signal in the average plaquette observed on a $12^3 \times 24$ lattice at $\beta = 5.2$ and $\mu = 0.01$ with the Wilson plaquette gauge action in [1], the absence of the metastability here signals a dramatic improvement of the phase structure due to the DBW2 gauge action. The presence of metastability at $\mu = 0$ and the absence of it at $\mu = 0.01$ indicates the existence of a rather short first order phase transition line near the origin in the (μ_κ, μ)-plane. Of course, for a precise localization of the first order phase transition line a detailed study of the infinite volume limit is required, which is beyond the scope of this paper.

An important question is the minimal value of the pion mass $m_\pi^{\min}$ associated to the first order phase transition line. A precise definition of $m_\pi^{\min}$ could be the value of the infinite volume pion mass just at the position of the first order phase transition, defined by the equal depth of the two free energy minima in the infinite volume limit. To obtain this would be rather demanding. Although the volume dependence could be studied beyond our volume extension of $L \simeq 2.4\,\mathrm{fm}$, for instance on a $16^3 \times 32$ lattice, the precise comparison of the free energy minima would be quite difficult. An approximate determination of $m_\pi^{\min}$ can be obtained by requiring the equality of the pion mass in lattice units am_π in the two phases on our $12^3 \times 24$ lattices. For this a linear extrapolation of $(am_\pi)^2$ from the points on both sides of the phase transition can be considered. As shown in the upper left panel of Fig. 5, our result at $\mu = 0$ is $(am_\pi)^2 = 0.0881$. This implies, with the range of r_0 values given above, that $m_\pi^{\min} \simeq 251\,\mathrm{MeV}$ in the positive quark mass phase and $m_\pi^{\min} \simeq 374\,\mathrm{MeV}$ in the phase with negative quark mass.

The minimal charged pion mass at $\mu = 0.01$ is $m_\pi^{\min} \simeq 360\,\mathrm{MeV}$ (see the lower left panel of Fig. 5). This originates from the non-zero value of the twisted quark mass and not from the presence of a first order phase transition.

In the right panels of Fig. 5 the bare quark mass in lattice units is shown. The dashed lines are linear fits to the points with positive and negative quark mass, respectively. At zero twisted mass (upper panel) the metastability region near the first order phase transition is clearly displayed. At $\mu = 0.01$ (lower panel) the difference between the two dashed lines is smaller. This difference may be interpreted as a consequence of a cross-over in the continuation of the first order phase transition line. In the figure there is also a linear fit to all points shown (full line) which goes reasonably close to every point. The two dashed lines also give lower and upper bound estimates for the critical hopping parameter: $0.1661 \leq \kappa_\mathrm{cr} \leq 0.1689$.

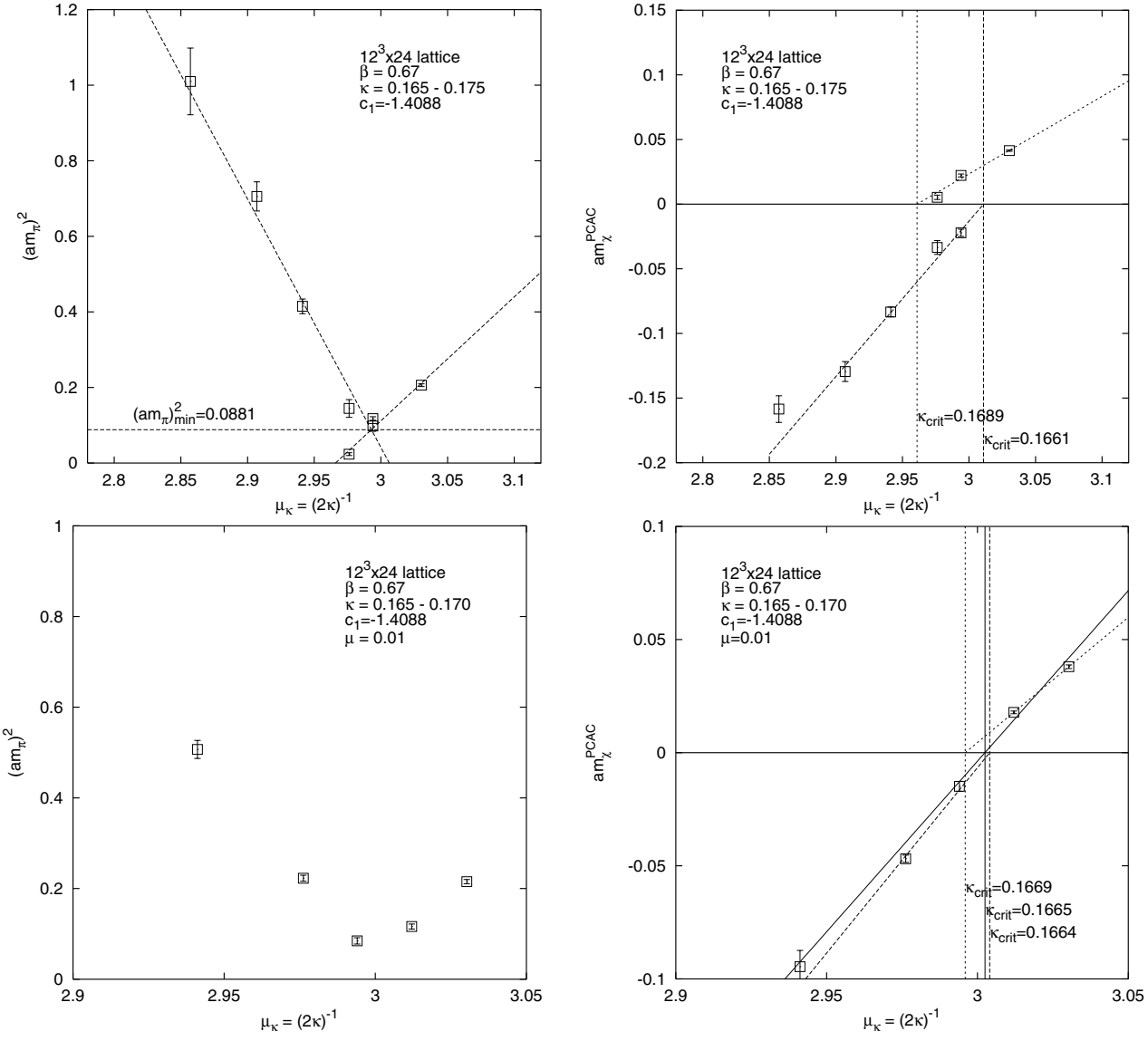

Fig. 5. Results of the numerical simulation on a $12^3 \times 24$ lattice at $\beta = 0.67$ as a function of $\mu_\kappa = (2\kappa)^{-1}$: upper panels $\mu = 0$, lower panels $\mu = 0.01$. Left panels: $(am_\pi)^2$, right panels: the bare PCAC quark mass am_χ^{PCAC}. The dashed straight lines are fits to the points in the positive and negative quark mass phase, respectively. The horizontal line in the upper left panel shows the estimated value of the minimal pion mass in lattice units. The straight lines in the right panels are explained in the text

Another way to estimate the critical hopping parameter (i.e. critical bare untwisted quark mass) is to determine the twist angle and find $\kappa_{\mathrm{cr}} = (2\mu_{\kappa_{\mathrm{cr}}})^{-1}$ where it equals $\pi/2$. Considering, for definiteness, the twist angle ω_V defined in Sect. 2.2, the fit in Fig. 6 gives $\kappa_{\mathrm{cr}} = 0.16651(2)$, in good agreement with the previous estimate. (Actually the numbers in Fig. 6 come from the vector Ward identity (13) but, within errors, (15) gives compatible results.) The Z-parameter appearing in this fit for ω_V is $Z_{oV} \equiv Z_A Z_S/(Z_V Z_P)$ (see Sect. 2.2 and [10]). According to Fig. 6 we have $Z_{oV} = 0.959(30)$. Since from an analogous fit to ω_A one could determine $Z_{oA} \equiv Z_V Z_S/(Z_A Z_P)$, this also offers a relatively easy way to obtain the Z-parameter combinations Z_A/Z_V and Z_P/Z_S.

The quantities $(r_0 m_\pi)^2$ and am_χ^{PCAC} can also be plotted against each other (see Figs. 7 and 8 for $\mu = 0$ and $\mu = 0.01$, respectively). Figure 7 and the data in Table 2 show that at $\mu = 0$, in the metastable region beyond the minimal pion mass, one can also reach values close to the physical value $m_\pi \simeq 140\,\mathrm{MeV}$.

3.3 Topological charge

The RGI gauge actions, and in particular the DBW2 action, are known to slow down the transitions between different topological sectors both in quenched [16] and in dynamical domain wall simulations [20]. In order to check this we determined the topological charge Q_{top} in some of

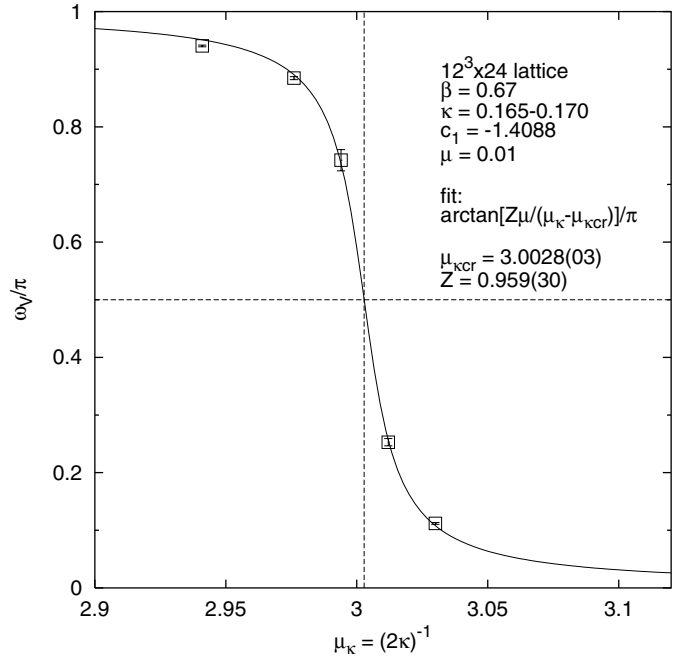

Fig. 6. The dependence of the twist angle ω_V on the bare untwisted quark mass $\mu_\kappa = (2\kappa)^{-1}$ at $\beta = 0.67$, $\mu = 0.01$ on a $12^3 \times 24$ lattice. The fit determines the critical hopping parameter to be $\kappa_{\rm cr} = (2\mu_{\kappa_{\rm cr}})^{-1} = 0.16651(2)$

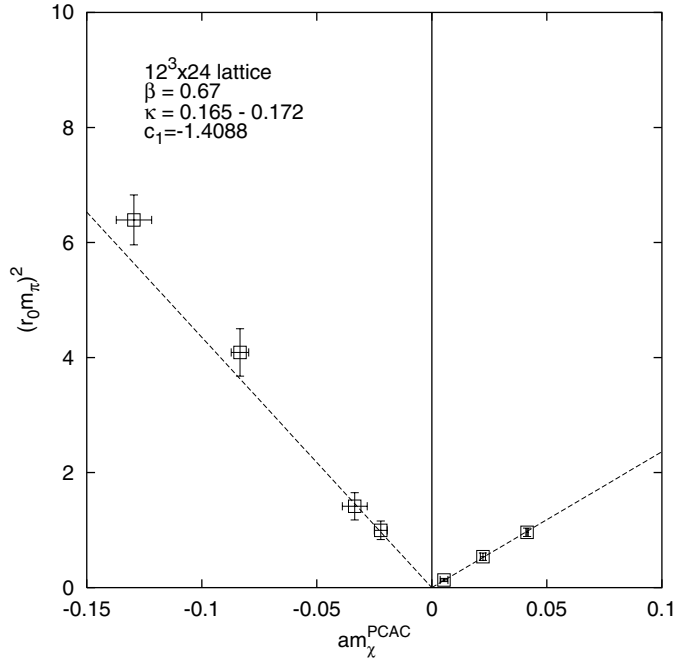

Fig. 7. The dependence of $(r_0 m_\pi)^2$ on $am_\chi^{\rm PCAC}$ at $\beta = 0.67$, $\mu = 0$ on a $12^3 \times 24$ lattice. The dashed lines are linear fits of the form $A|am_\chi^{\rm PCAC}|$. At the right all three points are included in the fit, at the left only two of them with the smallest quark masses. The fit parameter is for positive and negative quark mass $A = 23.6$ and $A = 43.5$, respectively

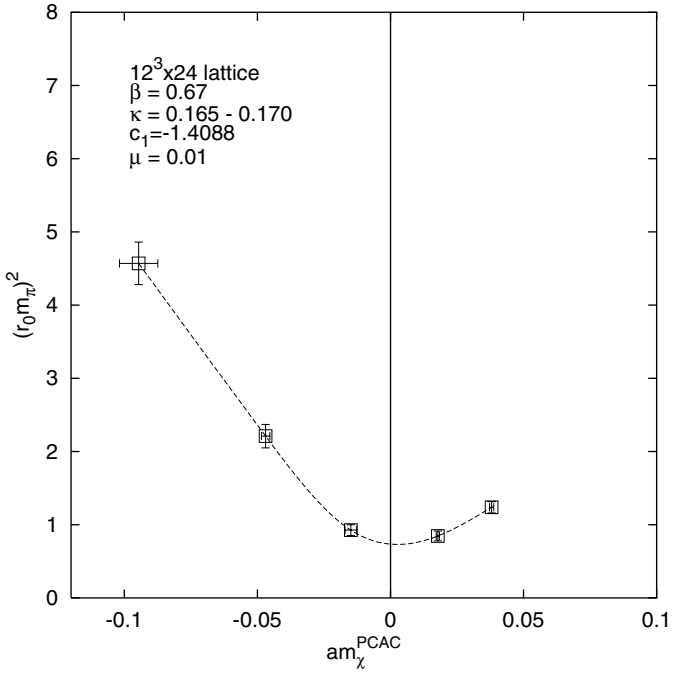

Fig. 8. The dependence of $(r_0 m_\pi)^2$ on am_χ^{PCAC} at $\beta = 0.67$, $\mu = 0.01$ on a $12^3 \times 24$ lattice. The dashed line is a spline interpolation for guiding the eyes

the runs using a cooling method [34]. In the following we denote the result from the cooling analysis by "topological charge", being aware of the fact that this definition contains some degree of arbitrariness. However, for our aim of testing the autocorrelation time this definition is sufficient.

In the run with label ($\mathcal{C}_{\rm h}$) ($12^3 \times 24$ lattice, $\beta = 0.67$, $\mu = 0.01$, $\kappa = 0.167$) the history of the topological charge is shown in the upper panel of Fig. 9. (The lower panel is a histogram of $Q_{\rm top}$.) The analyzed configurations are separated by 10 TSMB update cycles. In this point, according to Table 2, the quark mass is about $m_q \simeq 0.3\, m_{\rm strange}$ and the pion mass $m_\pi \simeq 380\,$MeV. As the figure shows, the topological charge is often changed. Its integrated autocorrelation in this run is $\tau_{\rm int}^{\rm top} \simeq 180$, but there is obviously a long tail of the autocorrelation which is not yet properly taken into account in a run of this length. In any case, $\tau_{\rm int}^{\rm top}$ is substantially longer than those of the average plaquette ($\tau_{\rm int}^{\rm plaq} \simeq 22$) or of the pion mass ($\tau_{\rm int}^{m_\pi} \simeq 6$) in Table 3.

In another run, the one with label ($C_{\rm l}$) ($12^3 \times 24$ lattice, $\beta = 0.67$, $\mu = 0$, $\kappa = 0.167$), where the quark mass is about $m_q \simeq 0.18\, m_{\rm strange}$ and the pion mass $m_\pi \simeq 295\,$MeV, the general picture is similar to Fig. 9. The integrated autocorrelation here comes out to be $\tau_{\rm int}^{\rm top} \simeq 70$, but this value is even less reliable because the run is shorter.

In spite of these relatively long autocorrelations, it is clear that in a sufficiently long run, say of length $1000\,\tau_{\rm int}^{m_\pi}$, which would be needed anyway for a good statistics on other quantities, the different topological sectors could be properly sampled by the TSMB algorithm. Therefore, at these bare parameter values, there is no problem with the

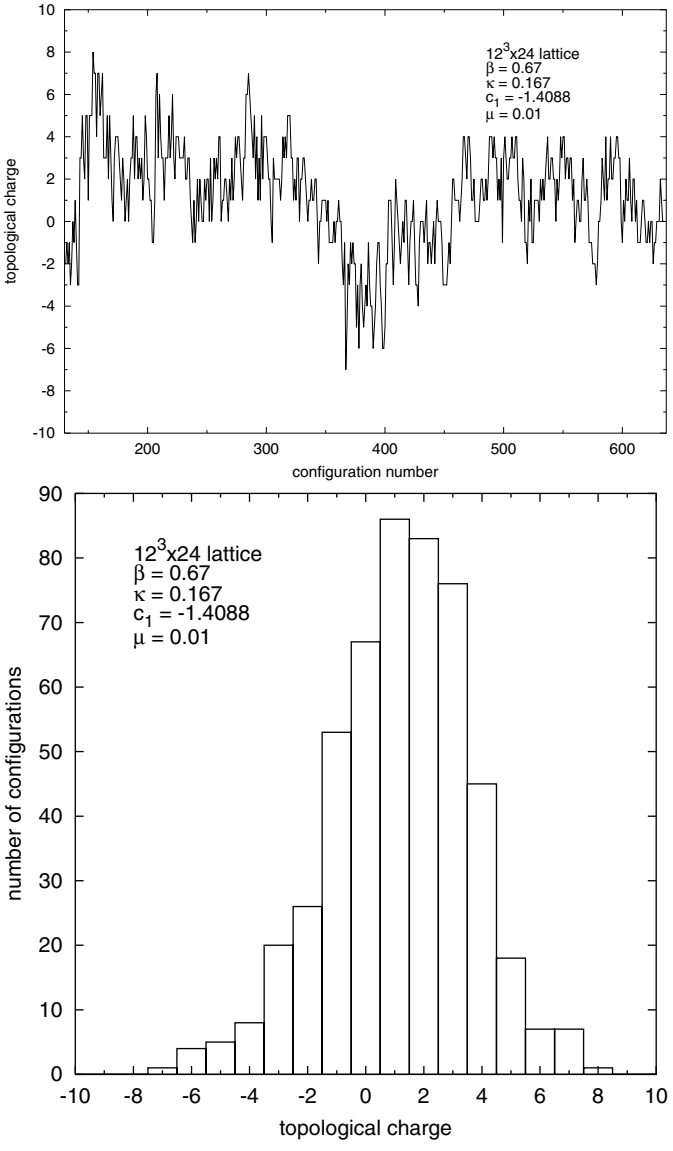

Fig. 9. The topological charge on a $12^3 \times 24$ lattice at $\beta = 0.67$, $\mu = 0.01$, $\kappa = 0.167$. Upper panel: the run history, with configurations separated by 10 TSMB update cycles. Lower panel: the distribution of the topological charge in this run

suppression of the transitions between different topological sectors.

3.4 Results about the update algorithm

In this paper we applied the TSMB update algorithm [26]. The estimates of the autocorrelations in different runs and the cost estimates obtained using (17) are given in Table 3. Since in our relatively short runs the autocorrelations can only be estimated, say, within a factor of two, the numbers in Table 3 give only a first orientation.

Qualitatively speaking, the $12^3 \times 24$ runs with "low plaquette" (positive quark mass) have lower costs than the corresponding runs with "high plaquette" (negative quark mass): at the same absolute value of the bare quark mass the runs in the negative quark mass phase have in most cases at least by an order of magnitude higher costs than those in the positive quark mass phase. The reason of the higher cost at negative quark mass is that the smallest eigenvalues fluctuate more frequently to very small values.

Table 3. The cost of an update cycle $C_{\rm cycle}$ in thousands of MVMs according to (17) and the estimated integrated autocorrelation lengths in update cycles obtained from runs specified by Table 1. The suffix plaq and m_π refer to the average plaquette and the pion mass, respectively. The last two columns give the factors F calculated from (19) with $z = 2$

run	$C_{\rm cycle}$	$\tau_{\rm int}^{\rm plaq}$	$\tau_{\rm int}^{m_\pi}$	$F_{\rm plaq}/10^6$	$F_{m_\pi}/10^6$
(a)	13	152		11.9	
(b)	19	100	20	3.5	0.7
(c)	30	147	< 5	1.3	< 0.04
(d)	48		12		0.001
(e)	65	167	< 5	24	< 0.7
(f)	38	95	9	33	3.1
(g)	25	32	< 5	9.5	< 1.5
$(A_{\rm l})$	19	21	< 5	0.8	< 0.2
$(C_{\rm l})$	29	18	15	0.3	0.3
$(C_{\rm h})$	50	53	33	1.5	0.9
$(D_{\rm l})$	51	77	< 5	0.1	< 0.01
$(D_{\rm h})$	51	113	7	7.8	0.5
$(E_{\rm h})$	43	61	11	22	3.9
$(F_{\rm h})$	30	56	< 5	33.4	< 3.0
$(G_{\rm h})$	31	52	6	48.4	5.6
$(\mathcal{A}_{\rm l})$	12	143	13	5.9	0.5
$(\mathcal{B}_{\rm l})$	21	41	9	0.6	0.1
$(\mathcal{C}_{\rm h})$	21	22	6	0.2	0.1
$(\mathcal{D}_{\rm h})$	21	72	8	7.8	0.9
$(\mathcal{E}_{\rm h})$	21	29	7	12.8	3.1

There is also a general tendency that the overall factors F decrease for decreasing absolute value of the quark mass. In fact, the data on F show that in the small quark mass region an inverse quark mass power $z = 1$ is a better approximation than $z = 2$, which has been observed in previous simulations with the Wilson plaquette gauge action [27–30,9]. At $\mu = 0$ the overall factor for the average plaquette $F_{\rm plaq}$ in the parameterization

$$C_{\tau_{\rm int}} \simeq F\,(am_q)^{-1}\,\Omega \tag{22}$$

turns out to be $F_{\rm plaq} \simeq 2 \cdot 10^7$ in the positive quark mass phase and $F_{\rm plaq} \simeq (2\text{–}3) \cdot 10^8$ at negative quark mass. The corresponding numbers at $\mu = 0.01$ are between these two values.

Let us note that at the smallest quark masses a final reweighting correction has to be applied because the smallest eigenvalues cannot be always kept in the interval of polynomial approximations. Sometimes they fluctuate below the lower limit ϵ.

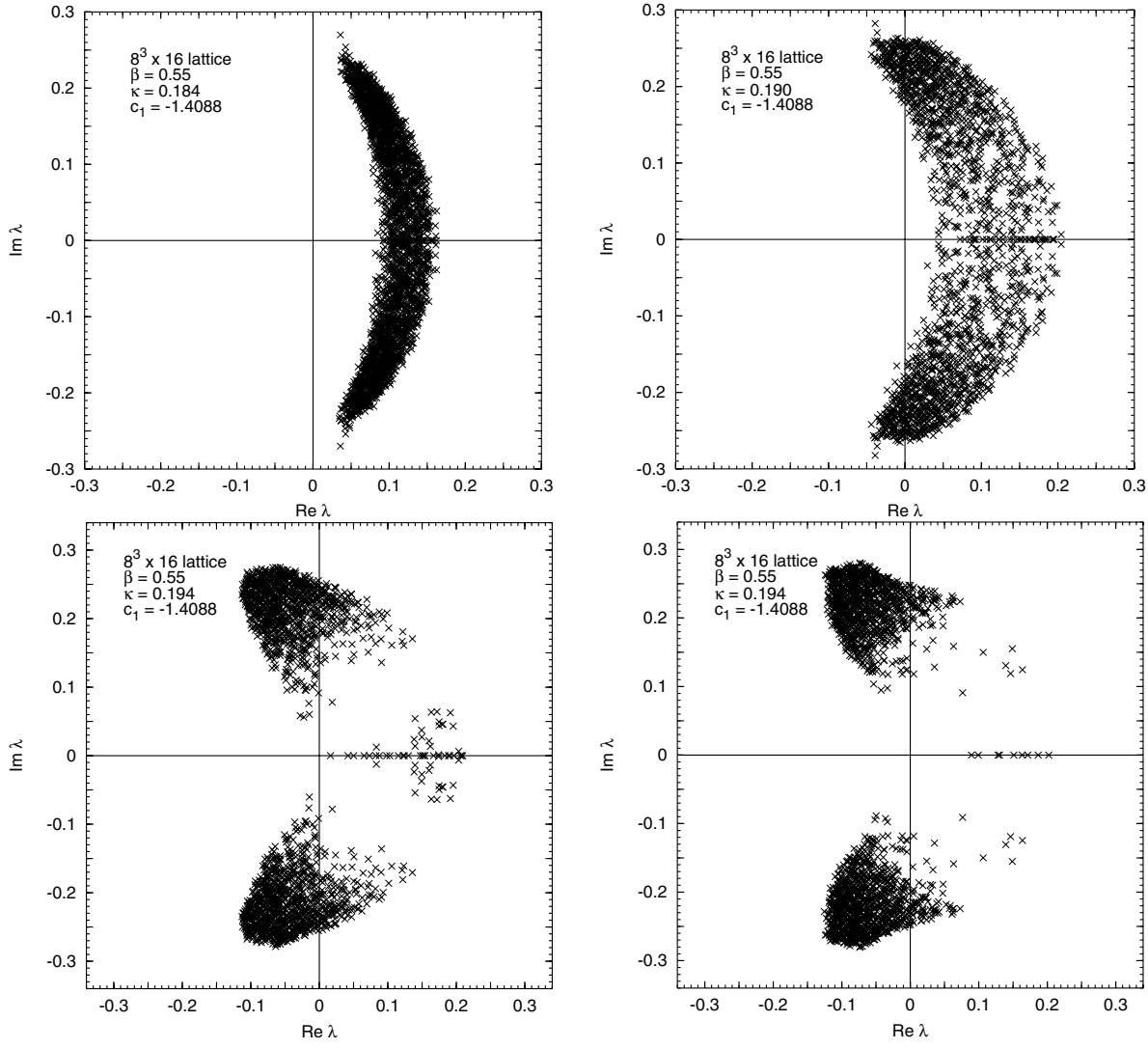

Fig. 10. Eigenvalues of the Wilson–Dirac fermion matrix (1) with small absolute value for $\mu = 0$, $\beta = 0.55$ on an $8^3 \times 16$ lattice. Upper left panel: $\kappa = 0.184$. Upper right panel: $\kappa = 0.190$. Lower panels: $\kappa = 0.194$ at the beginning of equilibration (left panel) and after equilibration (right panel)

4 Eigenvalue spectra

Looking at the eigenvalue spectra of the Wilson–Dirac fermion matrix (1) at small (untwisted) quark masses (see, for instance, in Sect. 4 of [27]) it seems plausible that near zero quark mass there has to be a massive rearrangement of eigenvalues. This is because in the path integral small eigenvalues are strongly supressed by the zero of the fermion determinant. At the sign change of the quark mass the eigenvalues have to somehow avoid the zero of the determinant at the origin. It is plausible that this eigenvalue rearrangement is related to the phase transition at zero quark mass.

An interesting question is how the behavior of eigenvalues in the small quark mass region is influenced by a non-zero twisted mass term.

We investigated the eigenvalue spectra by the Arnoldi method on $8^3 \times 16$ and $12^3 \times 24$ lattices in some of the runs listed in Table 1. Typically 100–200 eigenvalues were determined on 10–30 independent gauge field configurations. The parameters of the Arnoldi code were set for searching the eigenvalues with the smallest absolute value.

The results at $\mu = 0$ on an $8^3 \times 16$ lattice are shown by Fig. 10. In the upper panels of the figure, where the quark mass is positive, typical "half-moons" filled with eigenvalues can be seen, which correspond to the figures in [27]. At negative quark mass – in the lower part of Fig. 10 – an almost empty segment in the middle of the "half-moon" appears. Comparing the two figures at negative quark mass one can also see how this segment is gradually emptied during equilibration.

It is remarkable that even after equilibration there are some real ("zero-mode") eigenvalues on the positive axis. Our Arnoldi code did not find in these configurations any negative real eigenvalues. In addition, it is quite surprising that, apart from the empty segment in the middle,

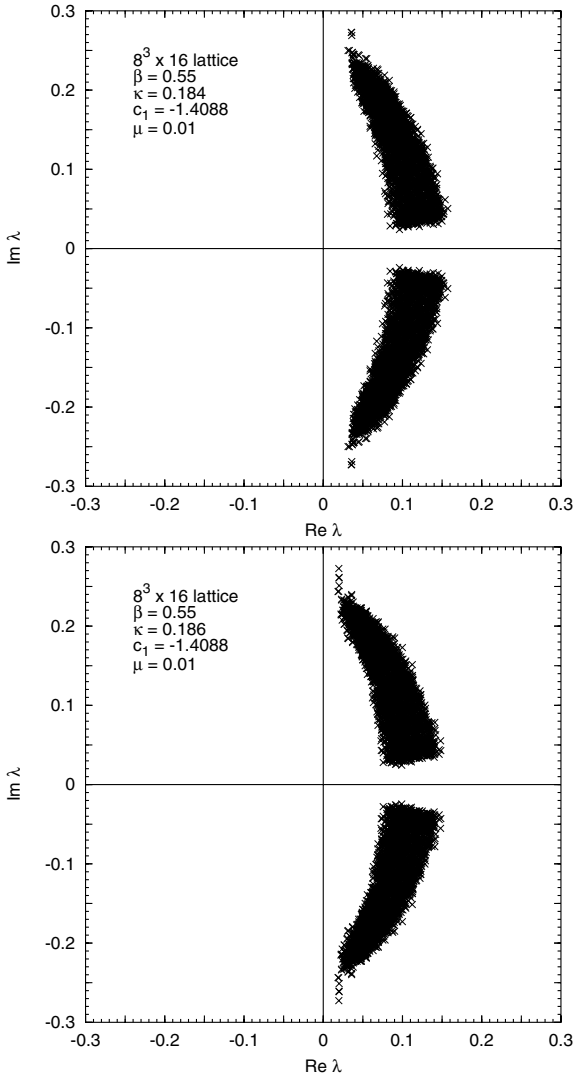

Fig. 11. Eigenvalues of the Wilson–Dirac fermion matrix (1) with small absolute value for $\mu = 0.01$, $\beta = 0.55$ on an $8^3 \times 16$ lattice. Upper panel: $\kappa = 0.184$, lower panel: $\kappa = 0.186$

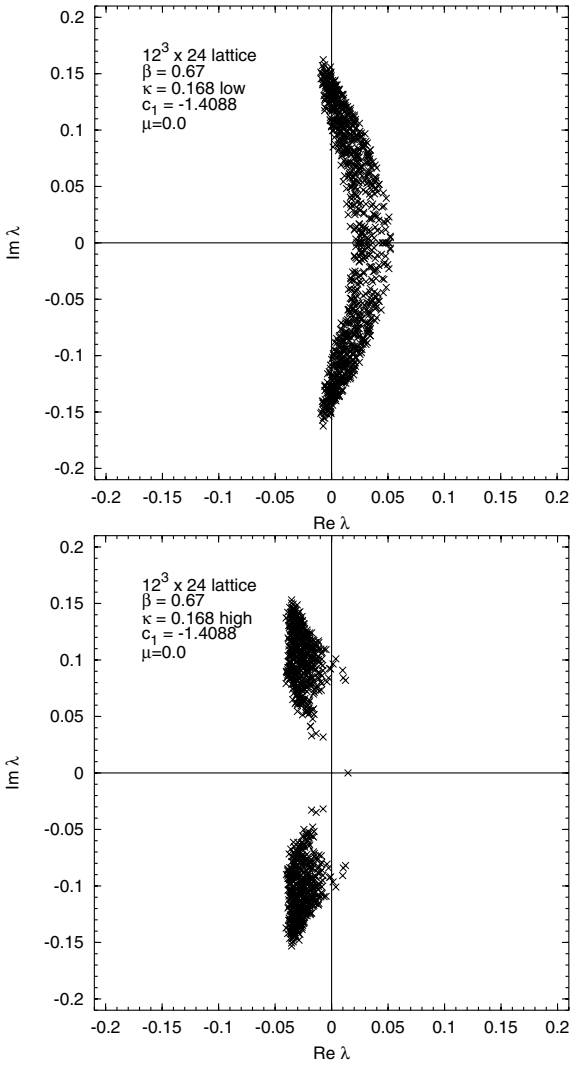

Fig. 12. Eigenvalues of the Wilson–Dirac fermion matrix (1) with small absolute value at $\beta = 0.67$, $\kappa = 0.168$ on a $12^3 \times 24$ lattice. Upper panel: $\mu = 0$, "low plaquette"; lower panel: $\mu = 0$, "high plaquette"

the half-moon-shaped deformation of the eigenvalue region observed at small positive quark masses does not disappear for small negative quark masses either.

The effect of a non-zero twisted mass on the eigenvalue spectrum on an $8^3 \times 16$ lattice is illustrated by Fig. 11. It can be seen that the strip around the real axis $-\mu \leq \mathrm{Im}(\lambda) \leq +\mu$ is free from eigenvalues. Let us remark that also in presence of a non-zero twisted mass we studied the spectrum of the operator of (1), which corresponds to the so-called "twisted basis". In the "physical basis" [35], for $\omega = \pi/2$, the spectrum of the Dirac operator lies in a vertical line parallel to the imaginary axis and is shifted from the origin by μ (exactly as in the continuum).

Going to larger β (smaller lattice spacing) the visible difference is that the "half-moons" are straightened and come closer to the origin; see Fig. 12. Otherwise most qualitative features are unchanged. There is, however, a marked difference in the number of real eigenvalues (for $\mu = 0$): in the upper panels of Fig. 10 there are lots of them, whereas at larger β, in the upper panel of Fig. 12, their number is substantially reduced.

The effect of changing the gauge action can be seen by comparing Fig. 12 with the eigenvalue spectra in case of the Wilson plaquette gauge action at a similar lattice spacing $a \simeq 0.2\,\mathrm{fm}$ in Fig. 13. The fact that in the case of using the Wilson gauge action the pion mass is larger than in the case of the DBW2 action is reflected by a movement of the "half-moons" farther away from the origin.

5 Conclusion

The main conclusion of this paper is that, indeed, exchanging the Wilson plaquette gauge action with the (renormalization group improved) DBW2 action shows substantial effects on the phase structure. We performed a qualitative

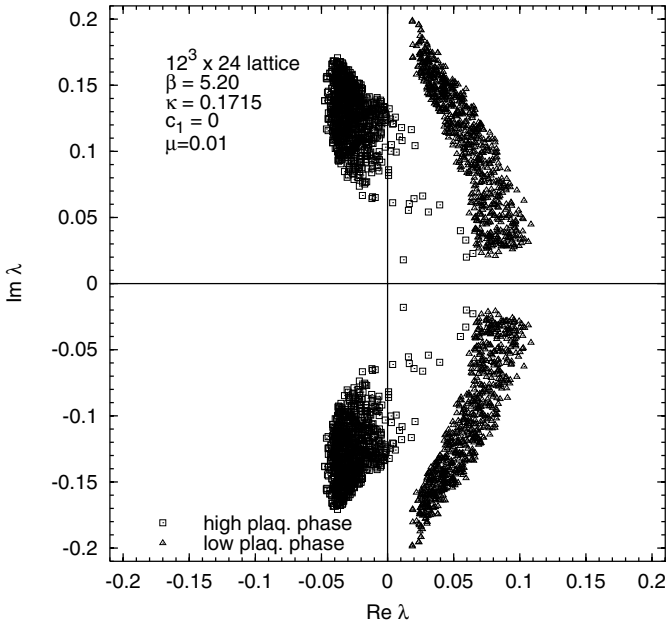

Fig. 13. Eigenvalues of the Wilson–Dirac fermion matrix with small absolute value in case of the Wilson plaquette action at $\beta = 5.20,\ \mu = 0.01,\ \kappa = 0.1715$ on a $12^3 \times 24$ lattice. Both "high plaquette" and "low plaquette" spectra are shown

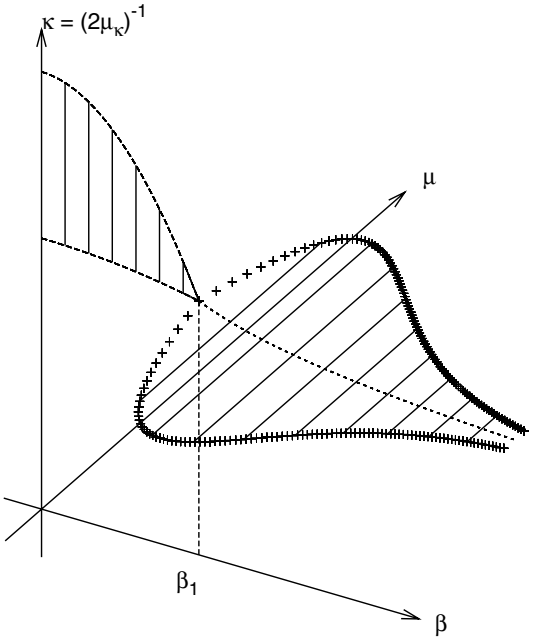

Fig. 14. The schematic view of the phase transitions in the (β, κ, μ) space for Wilson quarks with both DBW2 and Wilson plaquette gauge action (β is the bare gauge coupling, κ is the hopping parameter, μ is the bare twisted quark mass, and $\mu_\kappa \equiv (2\kappa)^{-1}$ is the bare untwisted quark mass.) The crosses mark the second order boundary line of the first order phase transition surface. At strong gauge coupling there is the surface containing the Aoki phase, which ends at a point denoted by $\beta = \beta_1$. The figure does not extend down to $\beta = 0$ and only one "finger" of the Aoki phase is shown

study of the phase structure of lattice QCD by changing the gauge action and compared the Wilson plaquette and DBW2 actions at a lattice spacing $a \simeq 0.2\,\mathrm{fm}$ in the positive quark mass phase and $a \simeq 0.17\,\mathrm{fm}$ in the phase with negative quark mass. This means: at $\beta = 5.2$ for the Wilson plaquette action and $\beta = 0.67$ for the DBW2 action. At this comparable situation the metastability signaled by the existence of long living states with different average plaquette value and quark masses with opposite sign becomes weaker and the minimal pion mass and the jump in the average plaquette between the phases with positive and negative quark mass decrease.

For vanishing twisted mass $\mu = 0$ the metastability occurs in the hopping parameter range $0.167 \leq \kappa \leq 0.168$. Going to the twisted mass value $\mu = 0.01$, which is the same as in the numerical simulations of [1,8], the metastability disappears on our $12^3 \times 24$ lattices. It might reappear on larger lattices, but our $12^3 \times 24$ data indicate that the jump in the average plaquette is at least by a factor of ten smaller than the one observed in [1].

At a lower β value, $\beta = 0.55$, which corresponds to lattice spacings $a \simeq 0.30\,\mathrm{fm}$ and $a \simeq 0.23\,\mathrm{fm}$ for positive and negative quark mass, respectively, our simulation data are consistent with the existence of the Aoki phase. This is similar to the situation for $\beta \leq 4.6$ in case of the Wilson plaquette action [33]. The schematic picture of the suggested phase diagram in the (β, κ, μ) space, both for DBW2 and Wilson plaquette gauge actions, is shown by Fig. 14.

The minimal pion mass in a stable phase can be estimated from our simulation data at $\beta = 0.67$ and vanishing twisted mass on a $12^3 \times 24$ lattice to be $m_\pi^{\min} \simeq 250\,\mathrm{MeV}$ in the positive quark mass phase and $m_\pi^{\min} \simeq 375\,\mathrm{MeV}$ in the phase with negative quark mass. On larger lattices this value is expected to be 10–20% smaller due to the finite volume effects which are non-negligible on the $12^3 \times 24$ lattice, especially in the negative quark mass phase where the lattice extension is only $L \simeq 2.0\,\mathrm{fm}$. At positive twisted mass $\mu = 0.01$ the estimate for the minimal charged pion mass is $m_\pi^{\min} \simeq 360\,\mathrm{MeV}$, a value entirely due to the non-zero twisted mass and not to the first order phase transition.

Besides the pion- and ρ-meson masses, at non-vanishing twisted mass, we also determined the twist angle ω_V as a function of the bare untwisted quark mass μ_κ. The μ_κ-dependence of ω_V can be well described by the expected arctan-function (see Fig. 6). From the fit one obtains the value of the critical hopping parameter $\kappa_{\mathrm{cr}} = 0.16651(2)$ and an estimate of a combination of Z-factors.

In some of the simulation runs we also monitored the history of the topological charge (see, for instance, Fig. 9). Although the autocorrelation of the topological charge is markedly longer than those of the average plaquette or of the pion mass, in a good statistics run with, say, thousand times the integrated autocorrelation length of the pion mass, the different topological sectors could be properly sampled.

In order to illustrate the rearrangement of the small eigenvalues near the zero quark mass phase transition we investigated in some detail the eigenvalue spectrum of the non-hermitean fermion matrix defined in (1). To our surprise, the transition from positive to negative quark mass is signaled in the eigenvalue spectrum by the opening up of an almost empty segment in the "half-moon" occupied by the eigenvalues near the origin. The introduction of a non-vanishing twisted mass causes the appearance of an empty strip $[-\mu, +\mu]$ on both sides of the real axis. The effect of larger β is to straighten the "half-moon" occupied by the small eigenvalues. At the same time the small real eigenvalues at zero twisted mass, which are causing the problem of the so-called "exceptional gauge configurations" in partially quenched simulations, occur much less frequently.

A welcome side-effect of introducing the RGI gauge action is the speed-up of the TSMB update algorithm. (This presumably also applies to other update algorithms, but in this paper we only used TSMB.) This can be qualitatively understood by the reduction of the probability for small size "dislocations" in the gauge field and for the less frequent occurrence of small real eigenvalues. (This is qualitatively similar to the conclusions of [36], obtained in another setup.) The computational cost as a function of the quark mass can be better approximated in the small quark mass region by an inverse power behavior of only $(am_q)^{-1}$ than by the behavior $(am_q)^{-2}$ observed previously with the Wilson plaquette action.

The results of the present paper indicate that the combination of $N_f = 2$ Wilson quarks with the DBW2 gauge action leads to a phase structure with a weaker first order phase transition than $N_f = 2$ Wilson quarks with the plaquette gauge action at a comparable value of the lattice spacing. For the moment we have no detailed information on the dependence of the phase structure on the parameter c_1 in the gauge action which multiplies the rectangular Wilson loops. It is possible that the optimal choice is different from $c_1 = -1.4088$, for instance, $c_1 = -0.331$ for to the Iwasaki action or $c_1 = -1/12$ for the tree-level improved Symanzik action. The best choice of c_1 might also be influenced by the positivity problem of improved actions [31] and/or by the convergence rate of lattice perturbation theory [37].

An important open question, which remains to be investigated in the future, is the β-dependence of the phase structure for Wilson-type lattice fermions. It is expected that closer to the continuum limit the minimal pion mass and the jump in the average plaquette become smaller and finally, in the continuum, the first order phase transition line in the plane of untwisted and twisted quark mass shrinks to a first order phase transition point. The faster this actually happens the better it is for phenomenologically relevant numerical QCD simulations with Wilson-type quarks.

Another important question is whether the DBW2 gauge action in combination with Wilson twisted mass fermions shows a good scaling behavior. To this end, a simulation at a higher value of β than the one used here is necessary. For the scaling studies previous experience in the quenched approximation [38] will be very helpful. Both questions mentioned above are presently investigated by our collaboration.

Acknowledgements. We thank Roberto Frezzotti, Gernot Münster and Giancarlo Rossi for helpful discussions, Stanislav Shcheredin for giving us his cooling code as well as Silvia Necco and Urs Wenger for their advice and help in evaluating the scale parameter r_0.

The computations were performed on the IBM-JUMP computer at NIC Jülich and the PC clusters at DESY Hamburg, NIC Zeuthen, Forschungszentrum Karlsruhe, University of Münster and the Sun Fire SMP-Cluster at the Rechenzentrum - RWTH Aachen. This work was supported by the DFG Sonderforschungsbereich/Transregio SFB/TR9-03.

References

1. F. Farchioni, R. Frezzotti, K. Jansen, I. Montvay, G.C. Rossi, E. Scholz, A. Shindler, N. Ukita, C. Urbach, I. Wetzorke, Eur. Phys. J. C **39**, 421 (2005); hep-lat/0406039
2. S.R. Sharpe, R. Singleton, Jr., Phys. Rev. D **58**, 074501 (1998); hep-lat/9804028
3. S. Weinberg, Physica A **96**, 327 (1979)
4. J. Gasser, H. Leutwyler, Annals Phys. **158**, 142 (1984)
5. K. Symanzik, Nucl. Phys. B **226**, 187 (1983)
6. B. Sheikholeslami, R. Wohlert, Nucl. Phys. B **259**, 72 (1985)
7. S. Aoki, Phys. Rev. D **30**, 2653 (1984); Phys. Rev. Lett. **57**, 3136 (1986)
8. F. Farchioni, C. Urbach, R. Frezzotti, K. Jansen, I. Montvay, G.C. Rossi, E. Scholz, A. Shindler, N. Ukita, I. Wetzorke, Nucl. Phys. Proc. Suppl. **140**, 240 (2005); hep-lat/0409098
9. R. Frezzotti, P.A. Grassi, S. Sint, P. Weisz, Nucl. Phys. Proc. Suppl. **83**, 941 (2000); hep-lat/9909003
10. ALPHA Collaboration, R. Frezzotti, P.A. Grassi, S. Sint, P. Weisz, JHEP **0108**, 058 (2001); hep-lat/0101001
11. G. Münster, JHEP **0409**, 035 (2004); hep-lat/0407006
12. S.R. Sharpe, J.M.S. Wu, Phys. Rev. D **70**, 094029 (2004); hep-lat/0407025; Nucl. Phys. Proc. Suppl. **140**, 323 (2005); hep-lat/0407035
13. L. Scorzato, Eur. Phys. J. C **37**, 445 (2004); hep-lat/0407023
14. CP-PACS Collaboration, A. Ali Khan et al., Phys. Rev. D **63**, 114504 (2001); hep-lat/0007014
15. RBC Collaboration, K. Orginos, Nucl. Phys. Proc. Suppl. **106**, 721 (2002); hep-lat/0110074
16. Y. Aoki et al., Phys. Rev. D **69**, 074504 (2004); hep-lat/0211023
17. K. Jansen, K. Nagai, JHEP **0312**, 038 (2003); hep-lat/0305009
18. Y. Iwasaki, UTHEP-118 (1983), unpublished.
19. T. Takaishi, Phys. Rev. D **54**, 1050 (1996); QCD-TARO Collaboration, P. de Forcrand et al., Nucl. Phys. Proc. Suppl. **53**, 938 (1997); hep-lat/9608094
20. RBC Collaboration, C. Dawson, Nucl. Phys. Proc. Suppl. **128**, 54 (2004); **129**, 167 (2004); hep-lat/0310055; RBC Collaboration, T. Izubuchi, Nucl. Phys. Proc. Suppl. **129**,

266 (2004); hep-lat/0310058; L. Levkova, R. Mawhinney, Nucl. Phys. Proc. Suppl. **129**, 399 (2004); hep-lat/0309122
21. JLQCD Collaboration, S. Aoki et al., Nucl. Phys. Proc. Suppl. **106**, 263 (2002); hep-lat/0110088
22. JLQCD Collaboration, S. Aoki et al., hep-lat/0409016
23. A. Ukawa, Nucl. Phys. Proc. Suppl. **53**, 106 (1997); hep-lat/9612011
24. M. Creutz, Talk given at RHIC Summer Study 96; hep-lat/9608024
25. P. Weisz, Nucl. Phys. B **212**, 1 (1983); P. Weisz, R. Wohlert, Nucl. Phys. B **236**, 397 (1984)
26. I. Montvay, Nucl. Phys. B **466**, 259 (1996); hep-lat/9510042
27. qq+q Collaboration, F. Farchioni, C. Gebert, I. Montvay, L. Scorzato, Eur. Phys. J. C **26**, 237 (2002); hep-lat/0206008
28. qq+q Collaboration, F. Farchioni, C. Gebert, I. Montvay, E Scholz, L. Scorzato, Phys. Lett. B **561**, 102 (2003); hep-lat/0302011
29. qq+q Collaboration, F. Farchioni, I. Montvay, E. Scholz, L. Scorzato, Eur. Phys. J. C **31**, 227 (2003); hep-lat/0307002
30. qq+q Collaboration, F. Farchioni, I. Montvay, E. Scholz, Eur. Phys. J. C **37**, 197 (2004); hep-lat/0403014
31. S. Necco, Nucl. Phys. B **683**, 137 (2004); hep-lat/0309017
32. R. Sommer, Nucl. Phys. B **411**, 839 (1994); hep-lat/9310022
33. E.M. Ilgenfritz, W. Kerler, M. Müller-Preussker, A. Sternbeck, H. Stüben, Phys. Rev. D **69**, 074511 (2004); hep-lat/0309057
34. E.M. Ilgenfritz, M.L. Laursen, G. Schierholz, M. Müller-Preussker, H. Schiller, Nucl. Phys. B **268**, 693 (1986)
35. R. Frezzotti, Nucl. Phys. Proc. Suppl. **119**, 140 (2003); hep-lat/0210007
36. M. Della Morte, R. Hoffmann, F. Knechtli, U. Wolff, Nucl. Phys. Proc. Suppl. **140**, 862 (2005); hep-lat/0409005
37. QCDSF Collaboration, R. Horsley et al., Nucl. Phys. B **693**, 3 (2004); hep-lat/0404007
38. K. Jansen, A. Shindler, C. Urbach, I. Wetzorke, Phys. Lett. B **586**, 432 (2004); hep-lat/0312013